

SQUID S700X

Papers

Parallel and Perpendicular Susceptibility Above T_c in $\text{La}_{2-x}\text{Sr}_x\text{CuO}_4$ Single Crystals
Pages 2 - 5

Anomalies in the relaxation of small magnetic particles at very low temperature
Pages 5 - 12

Parallel and Perpendicular Susceptibility Above T_c in $\text{La}_{2-x}\text{Sr}_x\text{CuO}_4$ Single Crystals

Gil Drachuck,¹ Meni Shay,^{1,2} Galina Bazalitsky,¹ Jorge Berger,² and Amit Keren¹

¹*Department of Physics, Technion - Israel Institute of Technology, Haifa, 32000, Israel*

²*Physics Unit, Ort Braude College, P.O. Box 78, 21982 Karmiel, Israel*

(Dated: January 25, 2012)

We report direction-dependent susceptibility and resistivity measurements on $\text{La}_{2-x}\text{Sr}_x\text{CuO}_4$ single crystals. These crystals have rectangular needle-like shapes with the crystallographic “c” direction parallel or perpendicular to the needle axis, which, in turn, is in the applied field direction. At optimal doping we find finite diamagnetic susceptibility above T_c only when the field is perpendicular to the planes. In an underdoped sample there is finite diamagnetic susceptibility above T_c in both field directions. The variations in the susceptibility data suggests a different origin for the fluctuating superconductivity above T_c between under and optimal doping.

The superconducting and ferromagnetic phase transitions share a lot in common, but it is simpler to visualize the order parameter of the latter. A ferromagnet produces a magnetic field only if all its domains are aligned. Similarly, a superconductor has no resistance only if the phase of the order parameter is correlated across the entire sample. However, there are temperatures high enough so that a ferromagnet has local magnetization, but without global alignment. Similarly, a superconductor can have local diamagnetism, without zero resistance across the sample. This situation is the hallmark of fluctuating superconductivity without global phase coherence. In a two dimensional system, where long range order is forbidden [1], the role of domains is played by a vortex anti vortex pair, which break the fabric of the phase.

In the highly anisotropic cuprates superconductors, the presence of diamagnetism well above the resistance critical temperature, T_c , was demonstrated some time ago, with high magnetic field H perpendicular to the superconducting planes [2]. This finding was, indeed, interpreted as persistence of finite order parameter amplitude throughout the sample, but with short-range phase coherence above T_c . However, a completely different interpretations could be offered to the same effect, in which electrons are inhomogeneously localized due to the randomness of the dopant. There are several experimental indication for inhomogeneously localization [3]. In this case superconductivity can occurs with finite order parameter amplitude only in three dimensional patches of the sample, leading to local diamagnetic signal without a continues resistance-free path at $T > T_c$. In the localization scenario, diamagnetic signal should be detected above T_c for all directions of the applied field H .

In this work, we examine the fluctuating superconductivity using magnetization (M) measurements of $\text{La}_{2-x}\text{Sr}_x\text{CuO}_4$ with the field parallel and perpendicular to the CuO_2 planes. We work in the zero field limit, as required from the definition of susceptibility. We also perform resistivity measurements on the exact same samples. Our major finding is a diamagnetic signal in the resistive phase of highly underdoped sample, for both par-

allel and perpendicular field supporting the localization scenario.

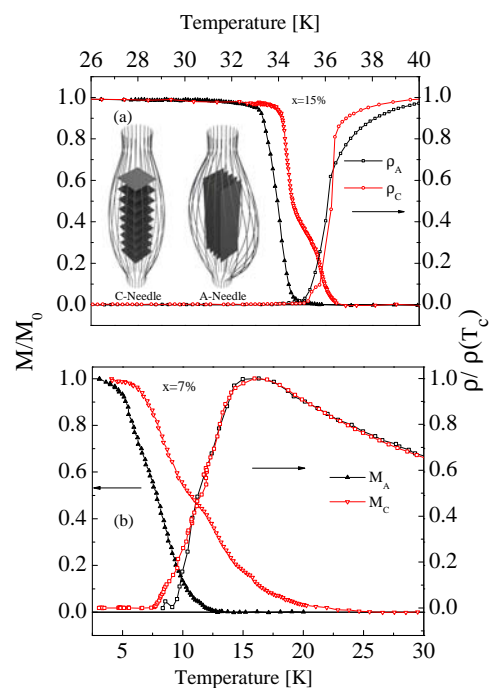


FIG. 1: LSCO normalized magnetization (left axis) and resistivity (right axis) measurements as a function of temperature of (a) optimally doped ($x = 15\%$) and (b) underdoped ($x = 7\%$) samples in an applied field of $H = 0.5$ Oe for two types of samples: A- and C-needles. In these needles the superconducting planes are parallel or perpendicular to the needle symmetry axis respectively. The magnetic field is applied along the needles. The A-needle is $1 \times 1 \times 10$ mm³ and the C-needle is $1 \times 1 \times 5$ mm³. M_0 is the magnetization at zero temperature and ρ_p is the resistivity at the peak. T_c^p indicates zero resistivity.

In magnetization experiments in the zero field limit, the measured susceptibility $\chi_m = \lim_{H \rightarrow 0} M/H$ depends on the sample geometry via the demagnetization factor (D), and is given by $\chi_m = \chi_i / (1 + D\chi_i)$ where χ_i is the intrinsic susceptibility. For needle-like samples, $D \simeq 0$

and $\chi_m = \chi_i$. Therefore, in order to determine χ_i properly needle-like samples are needed. To achieve the $D \simeq 0$ condition we use rod-like $\text{La}_{2-x}\text{Sr}_x\text{CuO}_4$ single crystals grown in an image furnace, which are oriented with a Laue camera and a goniometer. After the orientation, the goniometer with the rod is placed on a saw to cut the needles. Two configurations are cut as shown in Fig. 1. These crystals have rectangular needle-like shapes with the crystallographic “c” direction parallel or perpendicular to the needle axis. We were able to prepare 10 mm long A-needles and only 5 mm long C-needles. The field is applied also in the needle axis direction. For each sample we performed direction-dependent susceptibility and resistivity measurements. The measurements are done in zero field cooling conditions using a Cryogenic SQUID magnetometer equipped with a low field power supply with a field resolution of 0.01G. Prior to each measurement batch, the external field is zeroed with a Type I SC. After the measurement, the needles were chopped and T_c of each piece was tested to insure uniform T_c (see supplementary material).

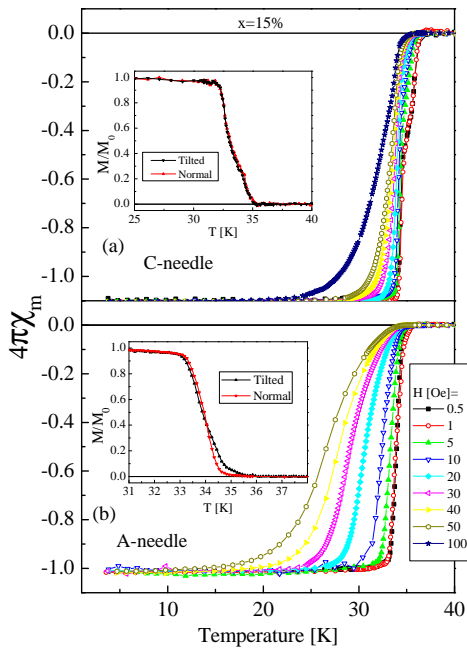


FIG. 2: The measured susceptibility χ_m ($\equiv M/H$) as a function of temperature for the 15% (a) C-needle and (b) A-needle in various magnetic fields. Insets: measurements of a straight and tilted needles demonstrating the effect of misalignment.

Figure 1(a) and (b) demonstrates our major finding. In this figure we depict the normalized magnetization M/M_0 as a function of T , at a field of $H = 0.5$ Oe, for the $x = 15\%$ and 7% samples respectively, for two different orientations. M_A and M_C are measurements performed on the A- and C-needle respectively. M_C shows

a knee just when M_A becomes finite. Resistivity data, normalized to 1 at the peak, are also presented in this figure; ρ_A and ρ_C are the resistivities measured with the corresponding needles with the contacts along the needles. The resistivity results are similar to those previously reported [4]. There is no observable difference in the critical temperatures defined as zero resistivity [T_c^p] as determined by ρ_A or ρ_C . In contrast, there is a clear anisotropy in the temperature at which the magnetization is detectable; this difference increases as the doping decreases. For the 15% sample: M_A is not detectable above $T_c^p = 35$ K, but M_C is finite up to 36.5 K. The critical temperature of the material T_c , could be defined by either T_c^p or by the presence of three dimensional diamagnetism (finite M_A). The strong residual M_C above T_c^p without residual M_A was never detected before in such low fields. It could result from decoupled superconducting planes disordered by vortices.

In contrast, for the 7% case, both M_A and M_C are finite at temperatures well above $T_c^p = 7.0$ K. M_A is not detectable only above 13 K and M_C is finite up to 25 K. The sharpest transition is observed with the M_A measurement and this type of measurement could be used to define doping and sample quality. The dramatic difference between the 15% and 7% doping indicates that the fluctuating superconductivity above T_c^p at low doping is fundamentally different from optimal doping, and could be derived by electronic inhomogeneous localization.

In order to verify these results we performed several control experiments. First we examine the influence of the field on the susceptibility. In Fig. 2 (a) and (b) we plot $4\pi\chi_m$ for the 15% C- and A-needles respectively, as a function of temperatures, and for several applied magnetic fields. For the field range presented, the saturation value of the susceptibility is field-independent. At $T \rightarrow 0$, $4\pi\chi_m = -1.1$ and -1.05 for the C- and A-needles respectively. For our rectangular C-needle, with dimensions of $1 \times 1 \times 5$ mm³, the demagnetization factor is $D \simeq 4\pi \times 0.09$, which explains well the measured susceptibility. For our rectangular A-needle with dimensions of $1 \times 1 \times 10$ mm³, $D \simeq 4\pi \times 0.045$ and we expect $4\pi\chi_m = -1.05$, which is slightly higher than the observed value [5]. A more accurate analysis of the susceptibility of needles is given below. At the other extreme, when $T \rightarrow T_c$ we see field-dependent susceptibilities but only for fields higher than 1 Oe. Below 1 Oe, $\chi_m(T)$ converges to a field-independent function representing the zero field susceptibility. Therefore, all our measurements are done with a field of 0.5 Oe. Finally, the knee exists in the $M_C(T)$ data only for fields lower than 10 Oe. Similar data for 7% is given in the supplementary material.

We also examined the relevance of misalignment of the samples to our results by purposely introducing a tilt of 7° to the 15% needles. The measurements of a straight sample and a tilted one are shown in the insets of Fig. 2. Tilt measurements for the 7% needles are given in the

supplementary material. Misalignment can lead to an error of 0.1 K per 1° in the estimate of the temperature at which the magnetization is null. This tiny effect cannot account for the difference in the magnetization between the A- and C-needles. In addition, the tilt make no different to the presence of the knee.

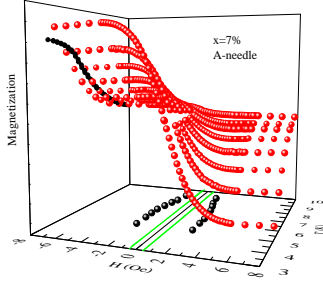


FIG. 3: A 3D plot of the magnetization as a function of magnetic field and temperature for the 7% A-needle. (floor): H_{c1} as a function of temperature. (wall): Magnetization as a function of T . The green solid line on the floor represents the applied field used in Fig. 1

Another concern is vortices. At a certain temperature close to T_c , the critical field H_{c1} must drop below the applied magnetic field and vortices can enter the sample. This puts a limit on the range of temperature where interpretation of our data is simple. Therefore, it is important to understand the behavior of H_{c1} near T_c . Figure 3 shows the results of $M(H, T)$ for $x = 7\%$ A-needle using a 3D plot. The values of H_{c1} are determined by fitting $M(H)$ to a straight line around $H = 0$ (not shown), and extracting the field where linearity breaks. $H_{c1}(T)$ is shown on the floor of the plot. The applied field, depicted as the straight green line on the floor, is lower than H_{c1} up to 12 K. At higher temperatures vortices can enter the sample.

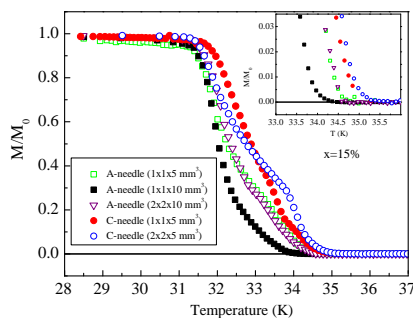


FIG. 4: Magnetization versus temperature for several 15% A- and C-needles with different sample dimensions. Inset: A zoom-in close to the transition temperature.

We also measured H_{c1} for the other samples (supplementary material). In particular, a field of $H = 0.5$ Oe is lower than H_{c1} for the 7% C-needle up to 20 K. This finding rules out the possibility that the knee observed in our C-needle measurements at fields lower than 10 Oe are due to lock-in/unlock-in transition of flux lines [6]. The knees of the 7% C-needle occurs at temperatures of 15 K at which the applied field is well below H_{c1} and no vortices exist in the sample. On the other hand, it is conceivable that the knee is a result of a transition between coupled and decoupled CuO_2 planes.

Finally, we investigated the impact of the sample geometry on the magnetization. The motivation here was to change the dimensions of the needles in terms of length-to-width ratio while maintaining needle-like aspect ratio. In Fig. 4 we present a multitude of 15% measurements for A- and C-needles. Similar data for the 7% samples are given in the supplementary material. The inset is a zoom close to T_c . The details of the magnetization curve are shape-dependent. However, the $2 \times 2 \times 10 \text{ mm}^3$ and $1 \times 1 \times 5 \text{ mm}^3$ A-needles have the same curve, demonstrating that the length-to-width ratio is the most important parameter. The closer the samples are to the ideal needle-like conditions, the bigger the difference in the magnetization between the two directions. This is, of course, expected since for a cubic or a spherical geometry, field lines cross the planes at an angle thus mixing the two susceptibilities leading to indistinguishable susceptibilities close to T_c [7].

All these tests support our observation that the magnetization of the A- and C-needle are fundamentally different by an amount larger than any possible experimental error. One might try to explain these differences as a finite size effect, namely, as the penetration depth diverges as $T \rightarrow T_c$ it might have a different values for each of the two different directions. Our magnetometer picks up a diamagnetic signal only when the penetration depth is similar to the sample width. This could occur at different temperatures, which are also different from T_c^p .

To address this possibility, we examined the London penetration depth (λ) in our 7% sample. In C-needle measurements, the screening currents run in the ab planes and the susceptibility is sensitive to the in-plane penetration depth λ_{ab} . In contrast, in the A-needle measurements, the screening currents run both in the plane and between planes. Therefore, the susceptibility is sensitive to both λ_{ab} and the penetration length between planes λ_c . To extract these λ 's we solve an anisotropic London equation

$$b_A - \lambda_{ab}^2 \frac{\partial^2 b_A}{\partial x^2} - \lambda_c^2 \frac{\partial^2 b_A}{\partial y^2} = 0 \quad (1)$$

$$b_C - \lambda_{ab}^2 \frac{\partial^2 b_C}{\partial x^2} - \lambda_{ab}^2 \frac{\partial^2 b_C}{\partial y^2} = 0 \quad (2)$$

with the boundary condition $b_\alpha = 1$, where b_A and b_C are the internal field divided by the applied field in the A- and C-needles respectively [8]. We define $\langle b_\alpha \rangle$ as the cross section average of b_α . For the A-needle we find

$$\langle b_A \rangle = \sum_{n \text{ odd}}^{\infty} \left\{ \frac{2/\sinh(\beta_n g) - 2/\tanh(\beta_n g) + \beta_n g}{jg^2 \beta_n^3 / 8} \right. \\ \left. + \frac{2/\sinh(\mu_n j) - 2/\tanh(\mu_n j) + \mu_n j}{jg^2 \mu_n^3 / 8} \right\} \quad (3)$$

where $g = w_y/\lambda_c$, $j = w_x/\lambda_{ab}$, $\beta_n = \sqrt{\left(\frac{\pi n}{j}\right)^2 + 1}$, $\mu_n = \sqrt{\left(\frac{\pi n}{g}\right)^2 + 1}$, and $w_{x/y}$ is the sample width taken as 1 mm. $\langle b_C \rangle$ is obtained from Eq. 3 by $\lambda_c \rightarrow \lambda_{ab}$. The susceptibility is given by $\chi_\alpha = (\langle b_\alpha \rangle - 1)/4\pi$. This provides an analytical solution for $\chi_C(\lambda_{ab})$ and $\chi_A(\lambda_{ab}, \lambda_c)$.

We obtain λ_{ab} by equating the analytical solution to the measured susceptibility of the C-needle. We then substitute this λ_{ab} into χ_A and extract λ_c by equating the analytical solution to the measured susceptibility of the A-needle. Figure 5 depicts the calculated $\lambda_{ab}(T)$ and $\lambda_c(T)$ for $x = 7\%$. Two arrows show the temperature where H_{c1} is on the order of our measurement field (0.5 Oe). Eq. 1 is valid at temperatures lower than indicated by the arrows. It is also clear that the magnetization is finite when the penetration depth reaches the sample's dimensions.

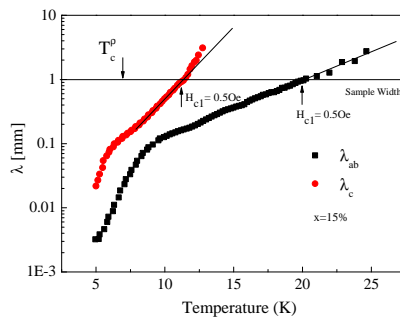


FIG. 5: A semi log plot of the penetration depths λ_{ab} and λ_c , for the 7% sample, as a function of T obtained by comparing the analytical solutions of Eq. 1 and 2 with the measured susceptibilities. The horizontal line represents the sample width. The points at which H_{c1} , for each needle, equals the applied field are also shown by arrows.

The surprising result is that λ_{ab} and λ_c run away from each other as the sample is warmed beyond T_c^p , and both reach the sample dimensions well above T_c^p . This means that if we could increase the thickness of our samples, while maintaining needle-like geometry, we would expect only larger difference between the temperature of zero magnetization and T_c^p , in contrast to a finite size scenario.

It is important to mention that there are other experimental works showing a strong anisotropy in the tem-

perature at which signals can be picked in LSCO [9]. In addition, it was recently suggested theoretically that two dimensional like superconductivity could be generated by frustration in the inter-layer coupling caused by stripes [10], or by c-axis disorder [11]. This could lead to two different magnetic critical temperatures.

To summarize, in this work we examined the anisotropy in the susceptibility of $\text{La}_{2-x}\text{Sr}_x\text{CuO}_4$ single crystals cut as needles. Our major findings are: I) diamagnetic susceptibility above T_c^p for $H \parallel \mathbf{c}$ at all doping, and in the zero field limit, II) diamagnetic susceptibility above T_c^p for both $H \parallel \mathbf{c}$ and $H \perp \mathbf{c}$ at low doping. We suggest that at low doping, electronic inhomogeneous localization is leading to local 3D superconducting patches, which provide diamagnetism without global superconductivity.

-
- [1] N. D. Mermin and H. Wagner, Phys. Rev. Lett. **17**, 1133 (1966).
 - [2] Y. Wang, L. Li, M. J. Naughton, G. D. Gu, S. Uchida, and N. P. Ong, Phys. Rev. Lett. **95**, 247002 (2005); Lu Li, Yayu Wang, M. J. Naughton, S. Ono, Yoichi Ando, and N. P. Ong, Europhys. Lett. **72**, 451-457 (2005); Lu Li, Yayu Wang, Seiki Komiya, Shimpei Ono, Yoichi Ando, G. D. Gu and N. P. Ong, Phys. Rev. B **81**, 054510 (2010).
 - [3] G. S. Boebinger *et al.*, PRL **77**, 5417 (1996); J. Hori, S. Iwata, H. Kurisaki, F. Nakanura, T. Suzuki, and T. Fuhita, J. Phys. Soc. Jpn. **71** (2002) 1346; S. Komiya and Y. Ando, PRB **70** (2004) 060503(R)
 - [4] S. Komiya, Y. Ando, X. F. Sun, and A. N. Lavtsov, Phys. Rev. B **65**, 214535 (2002). Y. Ando, S. Komiya, K. Segawa, S. Ono, and Y. Kurita, Phys. Rev. Lett. **93**, 267001 (2004).
 - [5] M. Sato and Y. Ishii J. Appl. Phys. **66**, 983 (1989).
 - [6] D. Feinberg *et al.*, Phys. Rev. Lett. **65**, 919 (1990); V. Vulcanescu *et al.*, Phys. Rev. B **50** 4139 (1994); P.A. Mansky *et al.*, Phys. Rev. B **52** 7554 (1995); Yu.V. Bugoslavsky *et al.*, Phys. Rev. B **56**, 5610 (1997); Y. Bruckental *et al.*, Phys. Rev. B **73**, 214504 (2006).
 - [7] C. Panagopoulos *et al.*, Phys. Rev. B **53**, R2999 (1996); A. Gardchareon, N. Mangkorntong, D. Hérisson, P. Nordblad, Physica C **439**, 85 (2006).
 - [8] Polyanin A D, 2002 Handbook of Linear Partial Differential Equations for Engineers and Scientists (London: Chapman and Hall).
 - [9] Q. Li, M. Hucker, G.D. Gu, A. M. Tsvelik, J. M. Tranquada, Phys. Rev. Lett. **99**, 067001 (2007); A. A. Schaffgans, A. D. LaForge, S. V. Dordevic, M. M. Qazilbash, W. J. Padilla, K. S. Burch, Z. Q. Li, Seiki Komiya, Yoichi Ando, and D. N. Basov, Phys. Rev. Lett., **104**, 157002 (2010).
 - [10] E. Berg *et al.*, Phys. Rev. Lett. **99**, 127033 (2007).
 - [11] P. Mohan, P. M. Goldbart, R. Naryanan, J. Toner, and T. Vojta, Phys. Rev. Lett **105**, 085301 (2010); D. Pekker, G. Refael, and E. Demler, Phys. Rev. Lett. **105**, 085302 (2010).

ANOMALIES IN THE RELAXATION OF SMALL MAGNETIC PARTICLES AT VERY LOW TEMPERATURES

SPEC report 96/058 (CEA Saclay)

To appear in the Proceedings of the "Magnetic Hysteresis in Novel Materials"

NATO Advanced Study Institute, Greece, July 1996

R. SAPPEY, E. VINCENT AND J. HAMMANN

e-mail : sappey@spec.saclay.cea.fr

*Service de Physique de l'Etat Condensé, CEA Saclay
91191 Gif sur Yvette Cedex, France*

F. CHAPUT AND J.P. BOILOT

*Groupe de Chimie des Solides,
Laboratoire P.M.C., CNRS URA D1254,
Ecole Polytechnique, 91128 Palaiseau, France*

AND

D. ZINS,

*Laboratoire de Physico-Chimie,
CNRS ER 44, Université Pierre et Marie Curie
4 place Jussieu, 75252 Paris, France*

Abstract. The magnetization relaxation rate of small $\gamma - Fe_2O_3$ particles dispersed in a silica matrix has been measured from 60 mK to 5 K. It shows a minimum around 150 mK, that can be discussed in terms of either thermal or quantum relaxation regime.

1. Introduction

The magnetization dynamics of single-domain nanometric particles at low temperature is presently a subject of intense interest, in the hope of finding evidence for quantum tunneling of the magnetic moment through the anisotropy barrier associated with the particle [1]. Apart from some pioneering attempts at a study of a unique particle [2], most efforts are concentrated on macroscopic samples, in which an accurate knowledge of the effective distribution of barriers is difficult, hence hindering a clear inter-

pretation of the results [3],[4]. Moreover, except in a few cases [5], the low-temperature range of the published data is often limited to pumped-He cryogenic techniques ($\sim 2K$), which still makes an unambiguous characterization of quantum effects more difficult.

In this paper, we present magnetic measurements which have been performed using a dilution refrigerator [7], that allow data to be taken down to $\sim 50mK$. We have studied a sample of $\gamma - Fe_2O_3$ particles, dispersed in a silica matrix, with a typical diameter of $\sim 6 nm$. The relaxation dynamics of $\gamma - Fe_2O_3$ particles has already been shown to exhibit some anomalies [8], that appear at the very end of the accessible temperature range (1.8 K). Our present data show that the relaxation rates in our sample do indeed fail to go down to zero when the temperature is lowered to 60 mK .

2. Sample characterization

The small particles of $\gamma - Fe_2O_3$ (maghemite) are embedded in a silica matrix, obtained by a polymerization process at room temperature. They are diluted to a volume fraction of 4.10^{-4} , in order to have them as independent as possible. The diameter distribution obtained by transmission electron microscopy is shown in the inset of Fig. 1; it can be fitted to a log-normal shape with peak value $d_0 = 6.3 nm$ and standard deviation $\sigma = 0.25$.

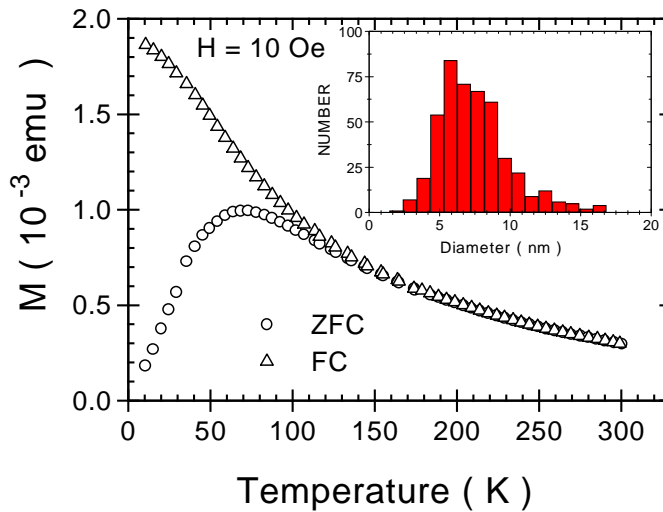


Figure 1. Total magnetic moment of the sample, measured in ZFC and FC procedures. The inset shows the size distribution of the particles deduced from transmission electron microscopy.

Fig.1 presents magnetic characterization measurements performed with a commercial SQUID magnetometer (Cryogenic Ltd). Here and all throughout the paper, we have plotted the measured magnetic moment in cgs units (corresponding to a total maghemite volume $\sim 4.10^{-5} \text{ cm}^3$). The “ZFC” curve is measured in the usual way by cooling the sample (down to 10 K) in zero field, applying a field and then raising the temperature; the field-cooled one (“FC”) is obtained while cooling in the field H .

The ZFC curve shows a broad maximum around $T^{peak} \simeq 73 \text{ K}$. It represents the progressive deblocking of larger and larger particles as the temperature T is raised. Let us consider that a particle of volume V involves an anisotropy barrier $U = K_a \cdot V$, where K_a is a density of anisotropy energy. If the time spent at a given T is t ($\sim 100 \text{ s}$), then for thermally activated dynamics most particles which are being deblocked at T have a typical volume V obeying an Arrhenius law

$$K_a \cdot V = k_B \cdot T \cdot \ln \frac{t}{\tau_0} \quad , \quad (1)$$

where $\tau_0 \sim 10^{-10} \text{ s}$ is a microscopic attempt time [9]. By assuming in addition that the saturated moment of a particle is proportional to its volume, and that the moments follow a Langevin function when they are deblocked (superparamagnetism), we have calculated the ZFC curve corresponding to the measured size distribution. The peak is obtained at the measured temperature for $K_a = 7.5 \cdot 10^5 \text{ erg/cm}^3$. This value is in agreement [10] with high-field measurements where the integral of the work needed for saturating the sample has been evaluated and also with Mössbauer spectroscopy results. It is one order of magnitude larger than the bulk maghemite value, as commonly observed in small particles where shape and surface contributions have increased the magnetic anisotropy [9].

Note that, due to the distribution width and to the $1/T$ variation of superparamagnetism, the ZFC-peak is found at a temperature which is three times larger than that corresponding to the peak value d_0 of the size distribution ($T_b(d_0) = 25 \text{ K}$) [10].

3. Magnetic behavior towards very low temperatures

The setup used for the low- T experiments is a home made combination of an r.f. SQUID magnetometer [6] and a dilution refrigerator [7]. The sample is coupled to the mixing chamber through a thermal impedance which allows a temperature range of 35 mK to 7 K. For relaxation measurements at the lowest temperatures, some spurious heating has been found when the field is varied, due to eddy currents in the thermalization link; we have therefore carefully adjusted the field amplitude, and chosen a “slow” cut-

off procedure (5 s), in such a way that the results become independent of both these parameters. We also have limited our lower range to 60 mK.

The sample is first cooled in zero field from room temperature to the dilution regime. From that point, the temperature can no longer be easily raised above 7 K. The procedure for the relaxation measurements at $T_0 \leq 5$ K starts with heating the sample to a high enough temperature for deblocking of all particles which may participate in the dynamics at T_0 , e.g. 7 K. Then the sample is field-cooled from 7 K to T_0 , the field is decreased to zero and the SQUID signal variation corresponding to the slow relaxation processes is measured. This procedure of not heating up to room temperature makes sense because our sample is highly diluted; in a first approximation the particles can be considered independent of each other. We have checked that our choice of the reinitialization temperature had no influence on the resulting dynamics.

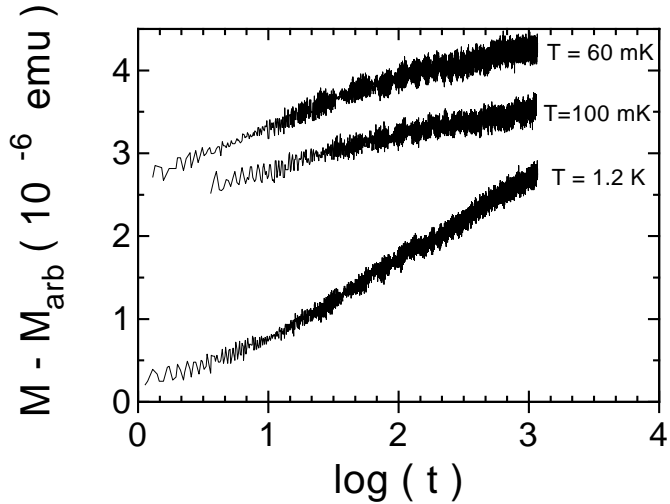


Figure 2. Typical relaxation curves at low temperatures, as a function of the decimal logarithm of the time in seconds. The curves have been vertically shifted by arbitrary values.

Figure 2 presents examples of relaxation curves. They are roughly logarithmic in time, apart from some uncertainty in the first seconds, which should be related to the 5 s field cut-off duration. In this paper, we only consider the average logarithmic slope of the curves (“magnetic viscosity”), which we determine between 10^2 and 10^3 s.

Figure 3 shows our set of results. For decreasing temperatures, the measured viscosity first decreases, then flattens out, and surprisingly increases

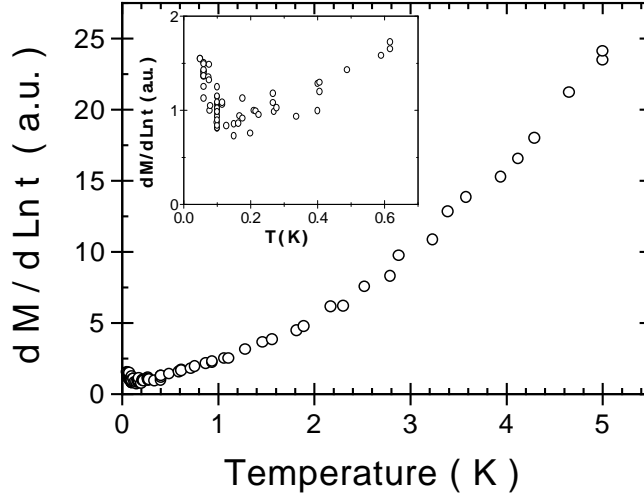


Figure 3. Magnetic viscosity as a function of temperature.

back below 150 mK. We present a simple model for the T-dependence of the viscosity before discussing this result in more detail.

4. A simple picture of thermal relaxation

By thinking of the sample relaxation at T as a sum of independent processes, one may write the total relaxing moment $M_T(t)$ as

$$M_T(t) = \int_0^{+\infty} m(U) P(U) \exp\left(-\frac{t}{\tau(U)}\right) dU \quad (2)$$

where the summation runs over the barrier distribution $P(U)$ associated with the size distribution of the particles. $m(U)$ stands for the “field-cooled moment” of the particles with anisotropy barrier U , which is the thermal average of the moments at their blocking temperature; as a first approximation, one may assume $U = K_a V$ and $m(U) \propto V$, hence $m(U) \propto U$. At any temperature T and after a time t following the field cut-off, one may consider that the only relaxing objects are those for which $\tau(U) = t$. The logarithmic derivative S of the magnetization (magnetic viscosity) can then be easily derived as

$$S \equiv \frac{\partial M_T}{\partial \ln t} \propto T \cdot P(U_c) \cdot m(U_c) \quad \text{where} \quad U_c = k_B \cdot T \cdot \ln \frac{t}{\tau_0} \quad . \quad (3)$$

The magnetic viscosity is commonly expected to be proportional to T [11], a controversial point since in our cases of interest the energy barrier dis-

tribution $P(U)$ may vary significantly [3],[4]. Indeed, from Eq. 3, one sees that the distribution of interest is $P(U).m(U)$ rather than $P(U)$ itself; with $m(U_c) \propto U_c$, Eq. 3 then becomes

$$S \propto T^2 \cdot \ln\left(\frac{t}{\tau_0}\right) \cdot P\left(U_c = k_B \cdot T \cdot \ln\left(\frac{t}{\tau_0}\right)\right) \quad . \quad (4)$$

We believe that these t and T^2 -dependences of the viscosity are probably hidden in most experimental results, due to the combination of the distributions $P(U)$ and $m(U)$ which are not accurately known (the $\ln^2(t/\tau_0)$ -variation of the magnetization is very close to $\ln t$, due to the microscopic value of τ_0). However, it seems to us that the first approximation of the viscosity in the case of non-interacting particles with a flat distribution of barriers should be a quadratic rather than a linear function of temperature.

5. Discussion

As expected from thermally activated dynamics and a regular distribution of barriers, the 0.5-5 K viscosity is seen to decrease for decreasing temperatures. It shows a slight upwards curvature which is compatible with a T^2 -dependence and a flat distribution; actually, this T-range corresponds to the blocking of 2-3 nm objects, which are not well characterized from the distribution in Fig.1. However, it is clear from Fig.3 that a normal extrapolation will not yield a zero viscosity at zero temperature; below 150 mK, the viscosity data even show a systematic tendency to increase as T is lowered. A similar behavior has been noted in an array of cobalt particles [12], and also in a Permalloy sample [13]. With respect to maghemite, a viscosity anomaly (plateau from 2.2 to 1.8 K) has been observed in a system of particles dispersed in a glassy matrix [8]; no anomaly was visible for the same particles in water, suggesting the influence of the matrix via magnetostriction phenomena [8].

We consider that our present results may give rise to two possible conclusions (a combination of both is also possible). First, one may assume that the dynamics is thermally activated. The implication of our results is that the distribution of energy barriers $P(U)$ increases abruptly towards smaller values, more rapidly than $1/U^2$. This is a surprising result, very different from the framework in which viscosity measurements are commonly interpreted in the literature (approximately a flat distribution). We have in addition performed ZFC/FC measurements in this low-T range, which are displayed in Fig.4. They show an increase in the magnetization for decreasing T, which is $1/T$ -like and of the same amount in both ZFC and FC cases (see TRM in Fig. 4). If this behavior is ascribed to clusters of e.g. 10 spins, the Curie constant would correspond to 0.5% of the total

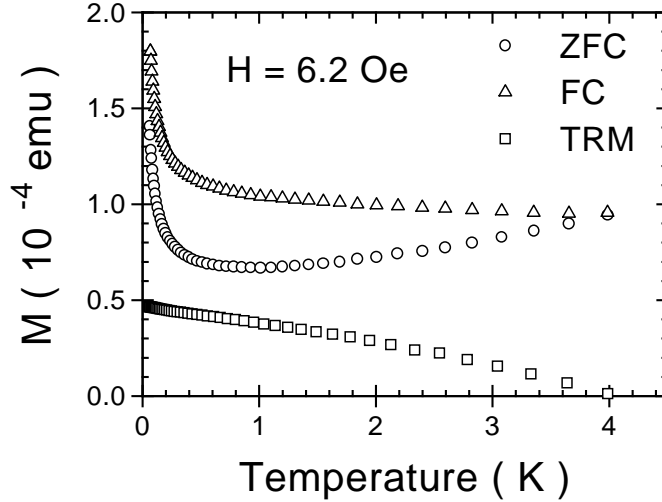


Figure 4. ZFC and FC curves in the low temperature region. The “TRM” curve has been measured when, after field-cooling to 60 mK, the field is cut and the temperature is raised. This measured TRM is equal to the difference between FC and ZFC, as usual when linear response theory applies.

$\gamma - Fe_2O_3$ amount. Thus, there are indeed some very small magnetic entities which are not frozen, even at 60 mK. Fig. 4 also shows a significant difference between the ZFC and FC curves, which corresponds to the slow dynamics observed in this low-T range. All data are therefore compatible with the existence of a significant low-energy tail of the barrier distribution, increasing further for the lowest values. One may think of very small particles; it would be of interest to check other systems of small particles for this possibility. It has also been proposed that such small barriers arise from decompensation effects at the surface of the ferrimagnetic particles [14]; surface defects might be an intrinsic component of the dynamics of nanometric particles at very low temperatures.

A second possible conclusion concerns the quantum tunneling of the particle magnetization (QTM) through its anisotropy barrier. In a first approximation, the contribution of such processes could be independent of temperature; from [1], quantum processes should be of the same order of magnitude as thermal processes below a crossover temperature T_c , which can be here estimated as $T_c \simeq 100 \text{ mK}$ (T_c does not depend on the barrier height, which only influences the relaxation rates). It is therefore possible that such processes contribute significantly in our T-range (one may even wonder why they should not be visible). The increase of the viscosity towards lower T can be understood in two ways. On the one hand, it has been

argued in [13] that the viscosity should be T-independent if the two energy levels between which quantum tunneling occurs are sufficiently separated with respect to $k_B T$, whereas it should go like $1/T$ for quasi-degenerate levels, which could be our situation of low-field relaxations. A low-T increase of the viscosity in Permalloy has thus been described as quantum jumps of a Bloch wall between pinning sites of comparable energies [13]. In more general terms, on the other hand, one may think that lower temperatures decrease the coupling to phonons, therefore reducing the dissipation and enhancing quantum tunneling processes [15].

A “T.Lnt” plot has been proposed to help distinguish between thermal and quantum processes in size-distributed particles [4], but this is not possible with the present relaxation data, obtained by measuring only SQUID signal variation (and not the full value of the magnetization). Actually, the question of a satisfactory evidence of QTM processes in such systems remains controversial; however, we believe that the numerous observations of anomalies in the low-T dynamics of small particles lead us to the minimal conclusion that things are not as simple as we had thought.

References

1. E. Chudnovsky and L. Gunther, *Phys. Rev. Lett.* 60 (1988) 661.
2. W. Wernsdorfer, K. Hasselbach, D. Mailly, B. Barbara, A. Benoit, L. Thomas and G. Suran, *J.M.M.M.* 145 (1995) 33.
3. B. Barbara, L.C. Sampaio, J.E. Wegrowe, B.A. Ratnam, A. Marchand, C. Paulsen, M.A. Novak, J.L. Tholence, M. Uehara and D. Fruchart, *J. Appl. Phys.* 73 (1993) 6703.
4. E. Vincent, J. Hammann, P. Prené and E. Tronc, *J. Phys. I France* 4 (1994) 273.
5. B. Barbara, W. Wernsdorfer, L.C. Sampaio, J.G. Park, C. Paulsen, M.A. Novak, R. Ferré, D. Mailly, R. Sessoli, A. Caneschi, K. Hasselbach, A. Benoit and L. Thomas, *J.M.M.M.* 140-144 (1995) 1825.
6. The SQUID magnetometry has been designed and patiently tuned by M. Ocio, whom we also thank for stimulating scientific discussions.
7. The special-purpose dilution refrigerator has been designed and built in CEA-Saclay by P. Pari and Ph. Forget, with the help of L. Le Pape.
8. X.X. Zhang, R. Ziolo, E.C. Kroll, X. Bohigas and J. Tejada, *J.M.M.M.* 140-144 (1995) 1853.
9. see e.g. J.L. Dormann, *Revue Phys. Appl.* 16 (1981) 275, and references therein.
10. R. Sappey, PhD thesis (Orsay University, France), in progress.
11. R. Street and J.C. Wooley, *Proc. Phys. Soc. London Ser. A*62 (1949) 562.
12. J-E. Wegrowe, W. Wernsdorfer, L. Thomas, B. Barbara, A. Sulpice, K. Hasselbach, A. Benoit and D. Mailly, *Phys. Rev.* B53 (1996) 6536.
13. S. Vitale, A. Cavalleri, M. Cerdonio, A. Maraner and G.A. Prodi, *J. Appl. Phys.* 76 (1994) 6332.
14. R.H. Kodama, A.E. Berkowitz, E.J. McNiff Jr. and S. Foner, *Phys. Rev. Lett.* 77 (1996) 394.
15. E. Chudnovsky, private communication; A.J. Leggett, S. Chakravarty, A.T. Dorsey, M.P.A. Fisher, A. Garg and W. Zwerger, *Rev. Mod. Phys.* 59 (1987) 1.